Available online at www.sciencedirect.com

ScienceDirect

Procedia Engineering 103 (2015) 405 – 412

Procedia Engineering

www.elsevier.com/locate/procedia

The 13th Hypervelocity Impact Symposium

Multi-Shock Shield Performance At 14 MJ for Catalogued Debris

J. E. Miller[a,b]*, E. L. Christiansen[c], B. A. Davis[b], D. M. Lear[c], and J. –C. Liou[c]

[a] University of Texas at El Paso, 500 W. University Ave., El Paso, TX 79968
[b] Jacobs, NASA Johnson Space Center, 2101 NASA Parkway, Houston, TX 77058
[c] NASA Johnson Space Center, 2101 NASA Parkway, Houston, TX 77058

Abstract

As the orbital debris population continues to grow significant tangible threats to robotic and crewed spacecraft have risen greatly over the last decade. These threats are currently mitigated operationally; however, an understanding of engineered solutions is useful to consider with respect to the risks and costs of operational mitigation. To this end a multi-shock shield has been designed and tested to demonstrate what it takes to stop an object that fits the energy profile of catalogued debris. A 14.25 MJ hypervelocity impact test has been performed on an enhanced, multi-shock shield at orbital speeds at the Arnold Engineering Development Complex (AEDC). The projectile was a hollow aluminum and nylon cylinder with characteristic dimensions typical of catalogued debris. The AEDC test of the shield occurred without any issues, and the shield successfully stopped the 598 g projectile at a mass penalty of 10.35 g/cm^2.

Peer-review under responsibility of the Curators of the University of Missouri On behalf of the Missouri University of Science and Technology

Keywords: multi-shock shield, catalogued debris, fabric shield

Nomenclature

S1	linear slope of shock wave versus particle velocity
S2	quadratic slope of shock wave versus particle velocity (s/m)
C	intercept of shock wave versus particle velocity (m/s)
ρ	density (g/cm^3)
ρ_{00}	solid density (g/cm^3)

1. Introduction

The near Earth orbital debris environment has continued to evolve and grow since the beginning of space flight with a near tripling of the tracked environment at some altitudes just in the past seven years [1]. This tracked environment includes objects with dimensions of about 10 cm and larger; therefore, these objects are generally thought to be mitigated by operational debris avoidance maneuvers. These maneuvers are not without substantial cost and risk for some vehicles. Coupled with the costs and risks is that the conjunction analysis for the debris and the operational vehicle is difficult owing to various aspects of the flight environment at low Earth orbit [2]. As a consequence satellite operators are left with difficult decisions about how and when to make debris avoidance maneuvers, and in the case of the International Space Station, the realization of the conjunction can be too late and the crew is forced to shelter in-place in an attached re-entry vehicle [3].

One strategy for skirting the debris avoidance maneuver is to design a shield that can stop the more difficult objects to track near the 10 cm threshold. To this end a multi-shock shield has been designed and tested to demonstrate what it takes to stop an object that fits the energy profile of catalogued debris. The 14.25 MJ

* Joshua E. Miller. Tel.: +1-281-244-8093.
E-mail address: joshua.e.miller@nasa.gov.

Peer-review under responsibility of the Curators of the University of Missouri On behalf of the Missouri University of Science and Technology
doi:10.1016/j.proeng.2015.04.039

hypervelocity impact test used a 598 g projectile impacting approximately normal to a NASA supplied multi-shock shield at 6.905 km/s. The projectile used in this demonstration is a hollow aluminum and nylon cylinder with an outside diameter of 8.6 cm and length of 10.3 cm. This test has been performed in February 2014 at Arnold Engineering Development Complex (AEDC) in preparation for the joint United States Air Force and NASA DebriSat test conducted in the same year.

The AEDC test of the re-engineered multi-shock shield occurred without any issues, and the re-engineered NASA multi-shock shield successfully stopped the 598 g projectile and the accelerated shield material. In this paper the improved capability multi-shock shield will be discussed along with the analysis and the test of the article.

2. Materials & Methods

The test article is a modified type 2 multi-shock shield previously tested at approximately 7 km/s using a 1.7 cm diameter aluminum projectile. This multi-shock shield is the most capable shield ever produced by NASA in terms of stopping energy per unit mass of shield [4]. The original multi-shock shield used four walls of four fabric layers of Nextel AF62 fabric (0.4 g/cm^2 per wall) and a single wall of seven layers of Kevlar KM2 fabric (0.16 g/cm^2) to stop the debris. This multi-shock shield consists of four walls of twenty-two fabric layers of fiberglass 3784 blankets (1.8 g/cm^2 per wall) and a seven layer steel mesh (1.08 g/cm^2) in front of a double rear wall of two sets of forty-five layer Kevlar KM2 blankets (1.035 g/cm^2) as shown to scale in Fig. 1a. An image of the actual test article prior to testing is shown in Fig. 1b.

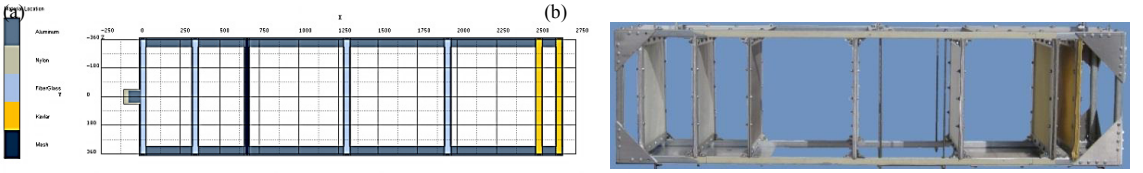

Fig. 1. Images of a 2.6 m multi-shock shield for the catalogued debris AEDC test (a) scaled computer generated drawing of the test article from hydrodynamic simulations (units in mm) and (b) photo of the test article with its support structure.

Looking from the left, where the projectile originates, to right in the figures, the first wall of the shield is made up of the layered fiberglass 3784 blankets. The second wall also of layered fiberglass 3784 blankets is 30 cm behind the first wall. The stainless steel mesh then follows the second wall of fiberglass by 30 cm. The third wall of fiberglass is 60 cm from the stainless steel mesh, which in turn, is followed by the fourth wall of fiberglass an additional 60 cm away. The rear walls of Kevlar are separated by 10 cm, and the separation between the fourth wall of fiberglass and the first Kevlar rear wall is 55 cm. The total length of the multi-shock shield, including wall thicknesses, is 2.65 m, and the shield has a total mass per unit area of 10.35 g/cm^2.

The projectile is a 598 g hollow cylinder of Al7075-T6511 closed on both ends as shown in the drawing of Fig. 2a. The spatial dimensions shown in the drawing are in inches and the angular dimension is in degrees. The aluminum inserts fit in a nylon case that acts as the sabot for the projectile that stays with the aluminum projectile throughout the flight to the multi-shock shield target. The photo of the actual projectile with the front insert separated from the cup insert is shown in Fig. 2b.

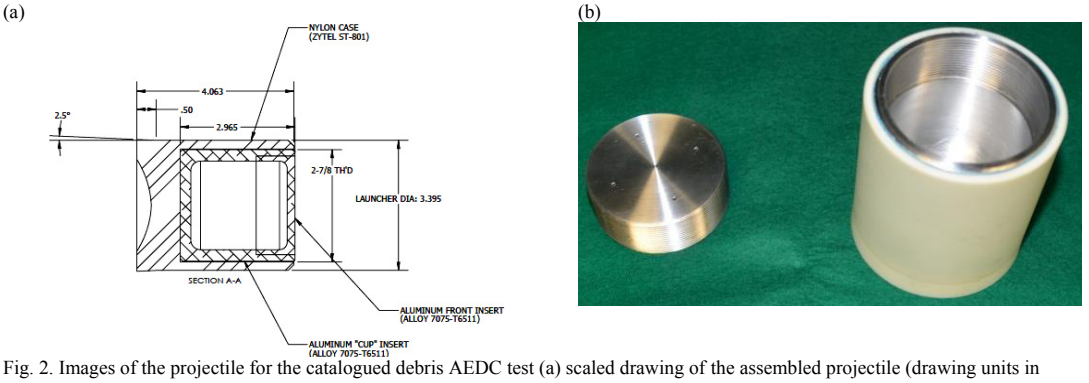

Fig. 2. Images of the projectile for the catalogued debris AEDC test (a) scaled drawing of the assembled projectile (drawing units in inches) and (b) photo of the projectile prior to mounting the front insert into the cup insert.

The acceleration system used for the impact test used the ballistic range G, two-stage, light-gas-gun at the Arnold Engineering Development Complex at the Arnold Air Force Base in Tennessee, United States [5,6]. The test used the 86 mm barrel capability of the range, where Fig. 3a and 3b show photographs of the target suspended in the target chamber using chains prior to the test. Prior to impact, high speed optical video of the projectile's flight and target impact is recorded for the test with a still from the test shown in Fig. 3c. In addition to the photographic evidence of the projectile, x-ray images have been obtained to verify the projectile integrity using three sets of orthogonal x-rays along the projectile's flight through the expansion chamber and the target chamber with a characteristic image nearest to the target shown in Fig. 3d. As can be seen in this x-ray image, the nylon back of the projectile separated from the aluminum cylinder in the flight of the projectile resulting in a double impact of the target. To ensure a clean test free of secondary piston debris from the acceleration of the projectile, the expansion chamber is isolated from the target chamber during the test by a guillotine mechanism after the projectile enters the target chamber and verified using optical video.

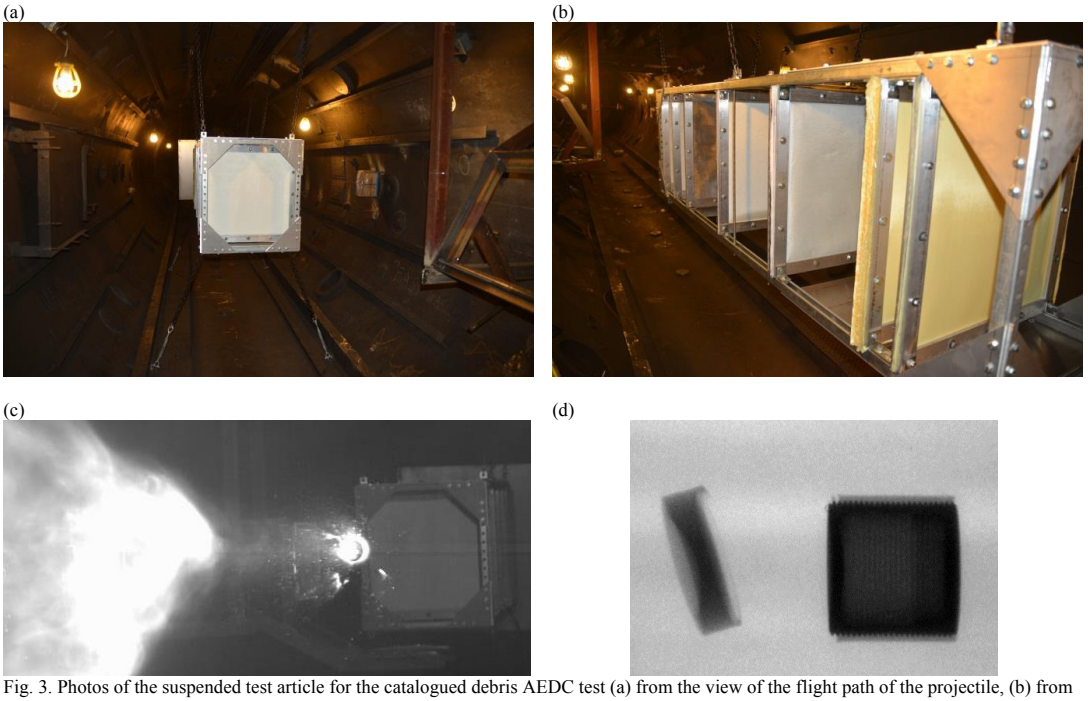

Fig. 3. Photos of the suspended test article for the catalogued debris AEDC test (a) from the view of the flight path of the projectile, (b) from the back of the target towards the target chamber entrance, (c) a still image from a video recording the projectile's flight to the target, and (d) an x-ray image of the projectile just prior to hitting the target.

3. Theory

Owing to the fact that the test conditions are well outside of previous experience with a multi-shock shield, a numerical analysis of the test has been performed prior to the test to modify the multi-shock shield design. The multi-shock shield initially assumed a geometrically scaled 5.4x TransHab multi-shock shield [7] as the foundation of numerical analysis efforts. From this initial shield, a series of two and three dimensional hydrodynamic simulations have been performed using the commercially available mechanical analysis code AUTODYN® to evolve the shield design. In all cases, the smooth particle hydrodynamics (SPH) solver native to AUTODYN® has been used to integrate the interaction of the projectile with the target through time. In this section the material and shield models are discussed for the shield considered at AEDC.

3.1. Analysis model properties

The material properties used with the modeling of the projectile are derived from the Al7075-T6511 and the nylon material models from the AUTODYN® material library [8] with the exception of an added material failure model for Al7075 based on the Grady spall model with the aluminum default critical strain value of 0.15. In both cases a Mie-Gruneisen extrapolation from the reference shock wave Hugoniot is used for the volumetric material response. The Al7075 deviatoric model uses the Steinberg-Guinan rate independent yield model for

modeling the plasticity; whereas, the nylon uses a rate independent von Mises yield surface. The nylon uses a simple minimum pressure to determine tensile failure of the material.

The soft product materials of the shield are not native materials of the AUTODYN® material library, and as a consequence had to be developed over the course of this work. The first soft product is fiberglass 3784 [9]. The fabric is untreated and uses an eight harness satin weave. The density of the fabric used in the analysis is determined from the vendor's guide values for mass per unit area of the fabric at 0.086 g/cm^2 and fabric thickness at 0.066 cm yielding an average density of 1.3 g/cm^3. The vendor's guide values for break strength of the fabric are 8,300 N/(5 cm) in warp and 7,000 N/(5 cm) in fill. In the analysis, it is assumed that the hydrodynamic tensile limit stress is determined from the midpoint of these break strengths and the thickness of the fabric yielding 230 MPa. As the fabric is in effect a porous silicate, the equation of state is interpolated from the various porosities of silica in the international shock wave database [10] shown in Fig. 4a in the shock wave strength versus compressed density plane relative to solid quartz at 2.65 g/cm^3. In addition to the data, the figure shows the projection of the loci of linear shock wave models for 1.55 g/cm^3 (S1 = 1.373 and C1 = 877 m/s in blue), 1.35 g/cm^3 (S1 = 1.386 and C1 = 678 m/s in orange) and 1.15 g/cm^3 (S1 = 1.404 and C1 = 409 m/s in green) [11,12] into the shock wave strength versus compression plane. Using these linear shock wave parameters, the interpolation of the shock wave parameters to 1.3 g/cm^3 yields a slope of 1.39 and an intercept of 618 m/s shown in red in the figure. As can be seen in the figure, the Hugoniot jump states for these porous materials are approximately on an isochor; therefore, the Gruneisen coefficient is approximately given by twice the slope of the jump states less unity yielding 1.78 for the 1.3 g/cm^3 silicate. In addition to these assumptions, this analysis also assumes that the bulk modulus, 497 MPa, is the same as the shear moduli corresponding to an effective Poisson ratio of 0.125 for the soft product.

A similar approach is used for the Kevlar fabric. The KM2 fabric is an untreated and plain weave aramid fabric [13]. The density of the fabric used in the analysis is determined from the vendor's guide values for mass per unit area of the fabric at 0.023 g/cm^2 and fabric thickness at 0.0305 cm yielding an average density of 0.755 g/cm^3. The vendor's guide values for break strength of the fabric are 7,700 N/(5 cm) in warp and 8,300 N/(5 cm) in fill, which in this analysis is interpreted as a hydrodynamic tensile limit of 526 MPa. As the international shock wave database [10] does not have aramids, this analysis used the porosity data from polyimide [14] shown in Fig. 4b to determine shock wave parameters of slope and intercept for 0.68 g/cm^3 (S1 = 1.303 and C1 = 681 m/s in blue), 0.48 g/cm^3 (S1 = 1.284 and C1 = 376 m/s in orange) and 0.32 g/cm^3 (S1 = 1.276 and C1 = 40.6 m/s in green). These shock waves parameters are extrapolated to 0.755 g/cm^3 yielding a slope of 1.302 and an intercept of 709 m/s shown in the figure as the red loci of shock wave states. Using the same assumptions as the fiberglass, the Gruneisen coefficient and the shear modulus are taken to be 1.604 and 380 MPa, respectively.

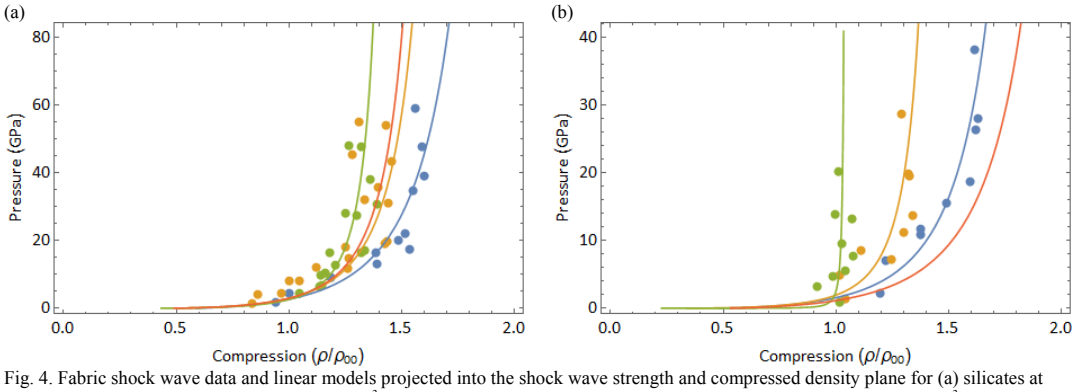

Fig. 4. Fabric shock wave data and linear models projected into the shock wave strength and compressed density plane for (a) silicates at initial densities of 1.55, 1.35 and 1.15 g/cm^3 in blue, orange and green, respectively with the interpolation for 1.33 g/cm^3 in red and (b) polyimide at initial densities of 0.68, 0.48 and 0.32 g/cm^3 in blue, orange and green, respectively with the extrapolation for 0.755 g/cm^3 in red.

The woven stainless steel mesh used in the test has a mass per unit area of 0.153 g/cm^2 and a thickness of 0.115 cm yielding an average density of 1.33 g/cm^3. The break strength of the mesh has been determined from the true stress at break, 127±6 MPa, and a true strain at break of 0.37±0.2 by way of five tensile tests of 2.5 cm wide samples shown in Fig. 5a. Porous iron shockwave data shown in Fig. 5b is used to derive the second order shock wave parameters projected to the shock wave strength versus the compressed density plane for 3.37 g/cm^3 (S2 = 1.185E-04 s/m, S1 = 1.16 and C1 = 650 m/s in blue) [15,16], 2.69 g/cm^3 (S2 = 1.185E-04 s/m, S1 = 1.07 and C1 = 550 m/s in orange) [17,18] and 1.575 g/cm^3 (S2 = 1.185E-04 s/m, S1 = 0.86 and C1 = 380 m/s in green) [19,20]. These shock wave parameters are used to extrapolate to the effective density of the mesh, 1.33

g/cm^3, yielding a quadratic slope of 1.185E-04, a linear slope of 0.81 and an intercept of 340 m/s, which is shown in red for the loci of shock wave states. The Gruneisen coefficient is taken as 1.42 and is derived from the slope yielding the isochoric peak compression of 7.7 g/cm^3. The shear modulus of the steel mesh is derived from the bulk modulus of 154 MPa and the effective elastic modulus of 343 MPa yielding 152 MPa and in line with the assumptions for the fiberglass and Kevlar fabrics.

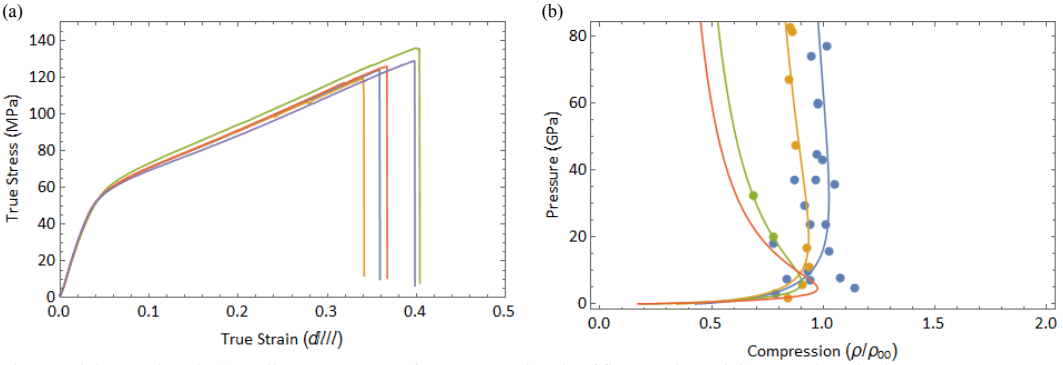

Fig. 5. Stainless steel mesh (a) tensile measurements of true stress and strain of five samples and (b) porous iron shock wave states at initial densities of 3.37, 2.69 and 1.575 g/cm^3 in blue, orange and green, respectively with the extrapolation for 1.33 g/cm^3 in red.

3.2. Pre-test shield design

Initial axially-symmetric, two-dimensional simulations considered the geometrically scaled 5.4x TransHab multi-shock shield. The simulations considered cylindrical walls of the multi-shock shield that matched the planned 360 mm wide by 20 mm thick walls equally separated by 600 mm. The two-dimensional SPH nodes in the simulations are 0.5 mm in width and height. To account for the open space between the layers of fabric composing a wall, every other layer of SPH nodes is removed from each of the walls prior to the simulation. As a result, each layer of nodes in the fiberglass walls is equivalent to one layer of fabric, and each layer of nodes in the rear wall is equivalent to two layers of Kevlar fabric. As a mechanism for adding margin to the preliminary analysis, the mass of the projectile in the sizing simulations is increased ten percent over the initial proposed mass of 670 g to 737 g yielding a designed to 18 MJ impact at 7 km/s. Altogether, the two-dimensional simulation uses 212,008 SPH nodes arranged as shown in Fig. 6 with 10,408 SPH nodes in the projectile. The simulated slice of the projectile and the shield are taken from the pre-impact state, Fig. 6a, through 800 μs, Fig. 6b. As can be seen, the analysis predicts penetration of the shield for the straight fabric multi-shock shield. In the case of the all fabric shield, the fabric alone did not disperse the projectile enough for subsequent layers to stop the remnants due to the cylindrical shape of the projectile.

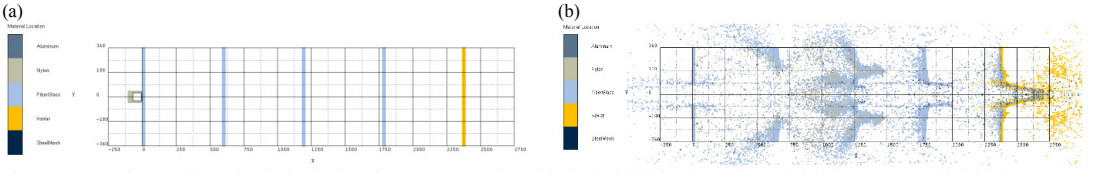

Fig. 6. Images of a two-dimensional simulation of a 5.4x TransHab multi-shock shield for the catalogued debris AEDC test (a) initial configuration of the problem and (b) integrated result of full penetration at 800 μs.

To enhance the multi-shock shield design to increase the dispersion, the second fabric wall of the multi-shock shield has been moved forward to the halfway point of the equally spaced walls, and in the place of the relocated wall a woven, stainless steel mesh has been introduced as can be seen in Fig. 7a. This arrangement allows the first two fabric walls to disrupt and expose the cylindrical walls of the projectile to the higher impedance steel mesh, which shreds the remaining solid aluminum. In addition to the steel mesh, the rear wall has been split in half and separated by 10 cm to spread the structural load, and the rear wall has been brought forward away from true equal spacing by 5 cm to fit the shield in the allocated test volume.

Axially-symmetric, three-dimensional simulations considered this multi-shock shield prior to the test. The simulations considered square walls of the multi-shock shield that matched the planned 360 mm wide by 20 mm thick walls. The three-dimensional SPH nodes in the simulations are 2 mm cubes. In addition to the shield

materials, the 6 mm aluminum structural frames are modeled to realize the appropriate boundary conditions. As with the two-dimensional simulations, layers of nodes are removed prior to the simulation to account for the open space between the layers; however, as a result of the larger node dimensions, each layer of nodes in the fiberglass and Kevlar walls are equivalent to four layers of fiberglass and eight layers of Kevlar, respectively. The three-dimensional simulation uses 2,084,322 SPH nodes with 12,522 SPH nodes in the projectile carrying the initial 18 MJ impact energy. The simulation has been taken through 7 ms,, as shown in Fig. 7b, where sequential images showed the rear wall to be stable with the shield stopping the advance of the debris.

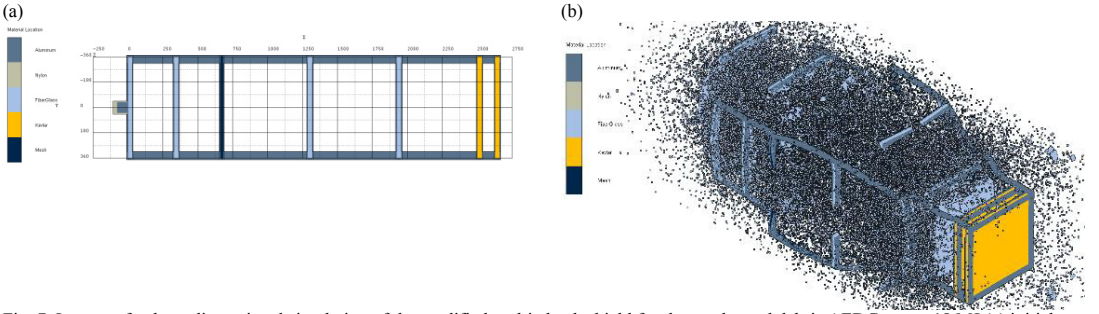

Fig. 7. Images of a three-dimensional simulation of the modified multi-shock shield for the catalogued debris AEDC test at 18 MJ (a) initial configuration of the problem and (b) back side of the shield at 7 ms.

4. Discussion

The test of the modified multi-shock shield design took place on 25 February 2014 at AEDC without any significant complications, and the shield successfully stopped the projectile, Fig. 8a. The first and second walls of fiberglass, Fig. 8b remained largely intact with a 130 mm diameter hole in the first wall and a 300 mm diameter hole in the second wall. With the displacement of these two holes it can be seen that the target is slightly pitched to the flight path by about 2 to 3°. As can be seen in Fig. 8a, the steel mesh has been almost completely removed from its frame; however, the frame did stay mounted to the support structure. The third fiberglass wall, also largely removed from its frame, became embedded in the fourth fiberglass wall. The last penetration of projectile material is into the fourth fiberglass wall. The final layer of fiberglass with a through hole in it is the thirteenth layer, Fig. 8c, with the fourteenth layer having scorch marks but intact, Fig. 8d. The fourth fiberglass wall with embedded third fiberglass wall impacted the rear wall causing only stretching damage and a tear in the fabric due to the frame of the fourth fiberglass wall, Fig. 8e. Significant structural loads occurred on the shield bending the channel and separating the framed wall material.

As can be seen from the success of the shield, the enhanced, multi-shock shield design did stop the 14.25 MJ, although, it stopped the impact quicker than *a priori* simulations predicted. Three significant features may account for the increased performance. First, the shield, initially designed for a projectile mass corresponding to 18 MJ, saw 20% lower impact energy than design. Second, the projectile shed part of the nylon back as can be seen in Fig. 3d, and while all of the material hit, it did not hit in the design sequence. Third, the shield had a 2° to 3° pitch relative to the projectile's flight path.

To determine the level of impact these three disparities have on the simulation of the shield, the three-dimensional simulations have been accomplished with the differences incorporated, Fig. 9a. Modifications made from the design analysis include switching from axially-symmetric to plane-symmetric simulations to account for a 2.5° pitch in the flight path. The rear nylon portion of the projectile is separated from the metallic portion of the projectile by 40 mm and pitched 15° from concentric with the projectile as seen in Fig. 3d. Finally, the extra mass and the adjustment to 6.9 km/s are made to reduce the impact energy to the tested 14.25 MJ impact energy. All other properties being equal to the design simulation, the posttest simulation uses 4,168,644 SPH nodes with 21,010 SPH nodes in the projectile carried out to 6.7 ms as shown in Fig. 9b where sequential evaluation shows the penetration status of the fourth fiberglass wall is not changing. As the impact remnants are embedded in the fourth fiberglass wall with no penetration, the differences in the design to and the actual test are sufficient to explain the higher performance of the enhanced, multi-shock shield design.

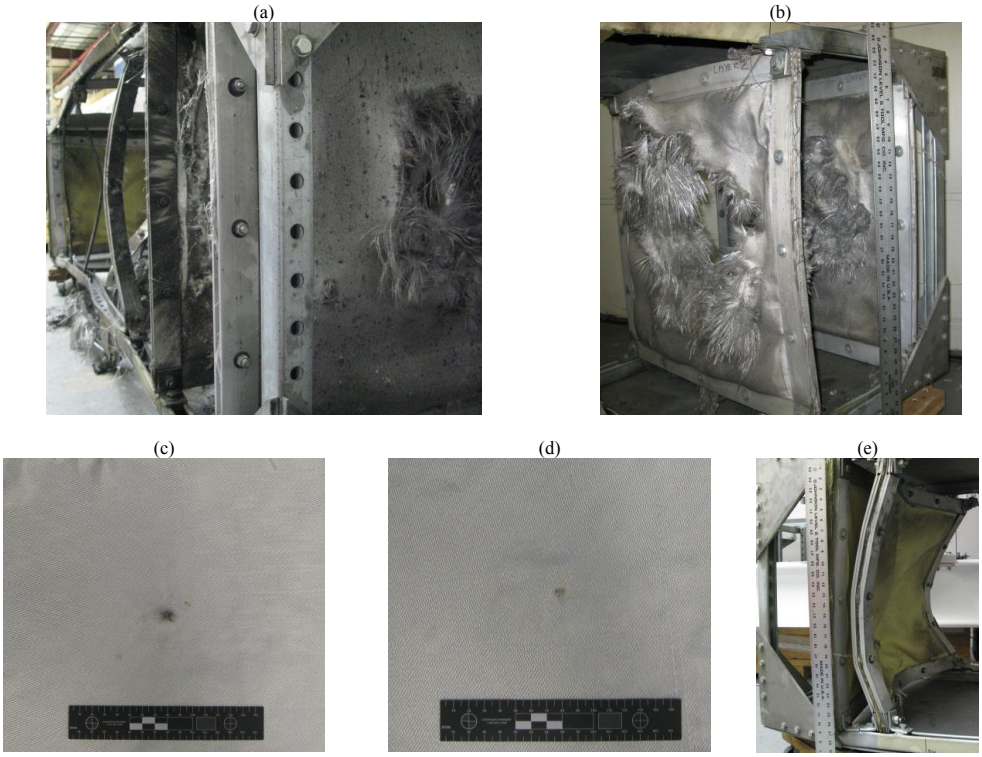

Fig. 8. Photos of the test article after the impact test (a) from the view of the flight path of the projectile through the entire article, (b) from the back of the first two layers, (c) the perforated thirteenth layer of the fourth wall, (d) the intact fourteenth layer of the fourth wall, and (e) a view of the two intact rear Kevlar walls.

5. Conclusion

An enhanced, multi-shock shield has been developed and tested to handle large debris of dimensions typical of the lower threshold of catalogued debris. The shield received thorough numerical analysis both prior and subsequent to its testing to understand the evolution of the threat as it progressed through the shield. The shield with a fielded mass per unit area of 10.35 g/cm^2 managed to stop a 598 g projectile with 14.25 MJ of kinetic energy with 0.8 g/cm^2. From the analysis work performed it is anticipated that the full 10.35 g/cm^2 shield could stop a 737 g projectile with18 MJ of kinetic energy.

Having a robust shield option like this demonstrates, that while challenging, mitigating sub-kilogram orbital debris is possible with mass penalties of order 10 g/cm^2; although, it is possible that expanding the parameter space to different material combinations may realize improved performance. In addition, this test also provides a unique validation point for the materials due to the scale of the test.

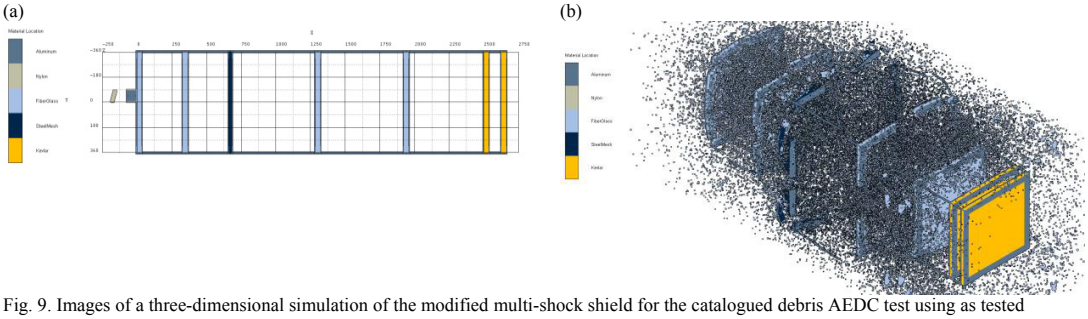

Fig. 9. Images of a three-dimensional simulation of the modified multi-shock shield for the catalogued debris AEDC test using as tested parameters (a) initial configuration of the problem and (b) back side of the shield at 6.7 ms.

The inclusion of the high impedance mesh is viewed as effective and critical to taking on the large array of material and shapes that may exist in orbit for this size regime. Future work considering the more varied potential shapes and densities is required to ensure that a satisfactory solution for deployment has been realized.

Acknowledgements

The authors wish to gratefully acknowledge the Arnold Engineering Development Complex for the seamless execution of this research in advance of the DebrisSat test, and the Hypervelocity Impact Technology group test team at NASA Johnson Space Center for the rapid development and delivery of the multi-shock shield.

References

[1] Liou, J. -C. (editor). “Increase in ISS debris avoidance maneuvers.” Orbital Debris Quarterly News, http;//orbitaldebris.jsc.nasa.gov/, 18, 2, 2014.
[2] Foster, J. L.and Wortham, W. B. ISS debris avoidance maneuver threshold analysis. NASA/TP-2007-214752, 1999.
[3] Liou, J. -C. (editor). Orbital Debris Quarterly News, http;//orbitaldebris.jsc.nasa.gov/, 16, 2, 2012.
[4] Christiansen, E. L., Kerr, J. H., De La Fuente, H. M., and Schneider, W. C. Flexible and deployable meteoroid/debris shielding for spacecraft. Prepared for the 1998 Hypervelocity Impact Symposium, 16-20 November 1998, Huntsville, AL, published in the International Journal of Impact Engineering, 23, 1999.
[5] Cable, A. J. Upgrade of the ballistic range facilities at AEDC: now complete. Prepared for the 18th AISS Aerospace Ground Testing Conference, 20-23 June 1994, Colorado Springs, CO, published in the AIAA Meeting Papers, AIAA-94-2493, 1994.
[6] Young, R. P. and Rushing, R. E. Expanded impact test capabilities of the Arnold Engineering Development Center. Prepared for the AIAA Space Programs and Technologies Conference, 24-26 September 1996, Huntsville, Al, published in AIAA Meeting Papers, A9641218, 1996.
[7] Dismukes, K. (curator). "TransHab Concept", S99-05362, http://spaceflight.nasa.gov/. Retrieved 2014-06-11.
[8] Autodyn Theory Manual, ANSYS – Century Dynamics, Cannonsburg, PA, November 2009.
[9] Style 3784 datasheet, BGF Industries, http://www.bgf.com/pages/data_sheet_detail/?fabric=1161&format=Metric. Retrieved 2014-02-15.
[10] Levashov, P. R. (curator). Shockwave database, http://www.ficp.ac.ru/rusbank/. Retrieved 2014-02-15.
[11] Trunin, R. F., Simakov, G. V., and Podurets, M. A. Compression of porous quartz by strong shock waves, Izv. Akad. Nauk SSSR. Fiz. Zemli 2, 33-39, 1971 [in Russian].
[12] Trunin, R. F. and Simakov, G. V. Compression of superporous silica in shock waves, Izv. Akad. Nauk SSSR. Fiz. Zemli 11, 72-79, 1990 [in Russian]
[13] Style 5705 datasheet, BGF Industries, http://www.bgf.com/pages/data_sheet_detail/?fabric=1326&format=Metric. Retrieved 2014-02-15.
[14] Bushman, A. V., Zhernokletov, M. V., Lomonosov, I. V., Fortov, Yu. N. and Khishchenko, K. V. Shock compressibility and equation of state of polyimide, Pis'ma Zh. Eksp. Teor. Fiz. 58(8), 640-644,1993 [in Russian].
[15] McQueen, R. G., Marsh, S. P., Taylor, J. W., Fritz, J. N. and Carter, W. J. The equation of state of solids from shock wave studies. - In: High Velocity Impact Phenomena / Ed. R.Kinslow. - New-York: Academic Press, p.293-417; appendies on pp. 515-568, 1970.
[16] Al'tshuler, L. V., Krupnikov, K. K., Ledenev, B. N., Zhuchikhin, V. I. and Brazhnik, M. I. Dynamical compressibility and equation of state for iron under high pressure, Zh. Eksp. Teor. Fiz. 34, 874-885,1958 [in Russian] (Sov. Phys. – JETP 7, 606-613, 1958).
[17] Trunin, R. F., Simakov, G. V., Sutulov, Yu. N., Medvedev, A. B., Rogozkin, B. D. and Fedorov, Yu. E. Compression of porous metals in shock waves, Zh. Eksp. Teor. Fiz. 96(9), 1024-1038,1989 [in Russian] (Sov. Phys. – JETP 69(3), 580-588, 1989).
[18] Trunin, R. F., Medvedev, A. B., Funtikov, A. I., Podurets, M. A., Simakov, G. V. and Sevast'yanov, A. G. Shock compression of porous iron, copper, and tungsten and their equation of state in terapascal pressure range, Zh. Eksp. Teor. Fiz. 95, 631-64, 1989 [in Russian] (Sov. Phys. – JETP 68(2), 356-361, 1989).
[19] Gryaznov, V. K., Fortov, V. E., Zhernokletov, M. V., Simakov, G. V., Trunin, R. F., Trusov, L. I. and Iosilevski, I. L. Shock compression and thermodynamics of highly nonideal metallic plasma, Zh. Eksp. Teor. Fiz. 114, 1242-1265,1998 [in Russian] (Sov. Phys. – JETP 87(4), 678-690, 1998).
[20] Trunin, R. F., Zhernokletov, M. V., Simakov, G. V., Gudarenko, L. F. and Gushchina, O. N. Shock compression of highly porous samples of copper, iron, nickel and their equation of state, Shock Compression of Condensed Matter - 1997, Prog. Am. Phys. Society Topical Group, Amherst, Massachussets, July 27 – August 1, 83-86,1998.